Numerical Methods in Civil Engineering

Journal Homepage: https://nmce.kntu.ac.ir/

Numerical Investigation of Wave Overtopping in Impermeable Seawalls Coated with Sand-Based Porous Media

Arefeh Emami*, Elaheh Elahian, Anant Parghi***, Meisam Qorbani Fouladi******

ARTICLE INFO

RESEARCH PAPER

Article history:
Received:
July 2025
Revised:
October 2025
Accepted:
November 2025

Keywords:
Seawalls
Porous media, Wave overtopping,
Numerical modelling, Sandstone layer

Abstract:

A seawall's structural integrity can be damaged by wave overtopping. To mitigate wave overtopping, this study investigates the effectiveness of incorporating a porous layer into impermeable seawalls. A numerical model wave was developed using a finite volume method and first validated by simulating an impermeable seawall without a porous layer, showing a 90% agreement with laboratory data. Applying a porous sandstone layer on the seaward face of the impermeable seawall followed this validation. A study was conducted to investigate the impact of various characteristics of the porous layer on the reduction of overtopping discharge, including thickness, porosity, and grain size. It was found that increasing the thickness of the porous layer (up to 2 m) resulted in a 60% reduction in overtopping discharge, while all other parameters remained constant. Moreover, increasing the porosity of the sand layer improved the reduction rate by 67%, indicating enhanced energy dissipation and absorption capacities. Using grain sizes of 0.2–1 mm and 2–3 mm reduces overtopping discharge by 35.57% and 66.2%, respectively. The results of this study demonstrate that the proposed approach is a viable and practical method of reducing wave overtopping.

1. Introduction

Marine engineers pay close attention to the infrastructure and properties of coastal regions. This focus stems from the fact that taking necessary precautions in this area can significantly protect people, investments, and nearby beaches. Seawalls are undoubtedly among the most important coastal protective structures. Built parallel to the shoreline, seawalls aim to protect the landward side from environmental phenomena. Therefore, analyzing the interactive effects of the structure and the surrounding environment is essential to meet the design objectives. Considering the continuous nature of water, which is generally regarded as the most significant load on structural faces.

* *Corresponding author: Assistant Professor, Department of Civil Engineering, Faculty of Engineering, University of Hormozgan, Bandar abbas, Iran. Email: emami@hormozgan.ac.ir*
** *MSc. Student, Department of Civil Engineering, Faculty of Engineering, University of Hormozgan, Bandar abbas, Iran.*
*** *Department of Civil Engineering, Sardar Vallabhbhai National Institute of Technology, Surat-395007, Gujarat, India.*
**** *Department of Civil Engineering, University of Science and Technology of Mazandaran, Behshahr, Mazandaran, Iran.*

When analyzing a structure's situation against waves, two aspects can be considered: wave-induced forces acting on the structure and hydrodynamic effects such as wave overtopping, which can impair the structure's performance and design objectives. This study specifically focuses on providing a solution to reduce overtopping. The extent of wave overtopping depends on various factors, including the wave climate and the geometry and materials used in construction [1]. Since accurately predicting and mitigating wave overtopping responses are fundamental challenges in the design process, this study focuses on hydrodynamic effects and presents a solution to reduce overtopping.

Considerable efforts have been dedicated to studying seawalls, with researchers focusing on predicting wave overtopping rates through experimental, empirical, and numerical models. Early studies primarily adopted experimental approaches, leading to the development of practical empirical equations to estimate overtopping rate on coastal structures ([2], Goda [3], van der Meer [4], Etemad-Shahidi, et al. [5], Pillai, et al. [6], Williams, et al. [7], Shaeri and Etemad-Shahidi [8], Chen, et al. [9], Cao, et al. [10]). In

https://doi.org/10.61882/NMCE.2507.1096

these studies, the overtopping rate has been evaluated in various configurations. Although empirical formulas help design and assess the hydrodynamic behavior of marine structures, conducting tests on small-scale physical models may lead to inaccurate results. Further, extrapolating empirical formulas may not always be appropriate, especially for complex configurations.

To overcome the deficiencies of empirical and experimental studies, it is therefore appropriate to use a flow model that was created using a numerical approach. Kobayashi and Wurjanto [11] extended the numerical model to predict monochromatic wave overtopping over the crest of a smooth impermeable structure. The average overtopping rates exhibited a commendable agreement with existing small-scale experimental data. Hubbard and Dodd [12] addressed wave run-up and overtopping of coastal structures through a 2D numerical model based on the 2D nonlinear shallow water equation. They employed a finite volume technique and a hierarchical Cartesian adaptive mesh refinement algorithm in their simulations. Xiao, et al. [13] conducted a numerical investigation into wave overtopping on a levee during Hurricane Katrina. Simulated wave conditions developed a numerical model for overtopping on sea dikes using Reynolds-averaged Navier-Stokes equations (RANS) and solitary wave run-up and overtopping on impermeable sloping seawalls at various water depths using a high-order Boussinesq-type model. Using a high-order Boussinesq-type model, Tsung, et al. [14] simulated solitary wave run-up and overtopping on impermeable sloping seawalls at various water depths. Their numerical model agreed with experimental data regarding run-up, run-down, shoreline position, and wave overtopping discharge.

Under the combined influence of extreme wave groups and wind, Yuan, et al. [15] studied the hydrodynamic stresses and overtopping mechanisms of a coastal barrier model on a sloped beach. Key effects include water depth, wind speed, and notable wave height. CHIWATA, et al. [16] emphasize an impermeable double parapet seawall as a countermeasure against storm surge flooding. Based on hydraulic tests for regular waves, the paper suggests an estimation equation to determine the wave overtopping discharge across the double parapet seawall. OpenFOAM was used in numerical tests to verify the relevance of the estimate equation under uneven waves. Pu and Shao [17] offer an incompressible smoothed particle hydrodynamics (ISPH) method to examine regular wave overtopping on coastal constructions of various kinds. The SPH method is a mesh-free particle modeling technique that can effectively handle the great deformation of free surfaces.

Chen, et al. [18] investigated wave overtopping at dikes using OpenFOAM as a 2D numerical model. They explored the effects of berms and roughness elements on reducing the average overtopping discharge at dikes. The OpenFOAM model results were validated with predicted wave overtopping and showed good accuracy. Even though several numerical studies have been conducted, these studies have focused on selecting a configuration that minimizes the overtopping rate.

A change in the geometry of the seawall may not be the only effective method for limiting the overtopping rate. The flow rate over a structure decrease as its height increases. passing over a structure is limited as its height increases. However, this solution increases the structure's size. It imposes a significant financial burden—one alternative approach is using porous materials, which have excellent energy dissipation capabilities in some engineering applications. Several researchers have investigated the interaction between waves and porous seabed or breakwaters, and a floating platform with porous media (e.g., [19-32]). Furthermore, Hieu and Vinh [33] numerically investigated wave overtopping of a seawall supported by a porous reef using a VOF-based two-phase flow model. In their study, the porous reef was located near the seawall with a terrace adjacent to the wall. They considered two optimum porosity values for the submerged reef, approximately 0.25 and 0.7, which yield minimum overtopping rates. Moreover, an effective porosity range of 0.4–0.65 was identified for the permeable terrace, leading to significant overtopping reduction. However, no studies have investigated the use of sand-based porous media in sea walls. While increasing surface roughness can indeed enhance energy dissipation, the mechanism is limited to turbulence generated at the surface. In contrast, a porous layer enables wave energy to penetrate and dissipate throughout the volume of the material via internal friction and viscous drag, resulting in significantly higher energy absorption. Furthermore, porous layers can be designed with tailored thickness, porosity, and grain size to achieve optimal performance under site-specific wave conditions. Therefore, this study introduces an innovative technique involving the application of porous layers to a battered impermeable seawall (BIS) and situates it within the current literature.

For this aim, this study numerically examines the performance of a BIS coated with sand-based porous layers to reduce wave overtopping discharge. Key porous-media parameters, including intrinsic permeability, layer thickness, and porosity, are extensively analyzed to determine their influence on wave energy dissipation and to identify configurations that optimize overtopping reduction. The study provides practical coastal engineering insights by numerically examining how porous-layer properties (thickness, porosity, and grain size) affect wave overtopping discharge, with results indicating that increasing thickness and adjusting porosity improve energy dissipation, reduce seawall deterioration, and decrease overtopping.

This study is structured as follows: Section 2 explores the geometrical aspects of battered impermeable seawalls covered with porous layers. A detailed description of the features and characteristics of the porous material is also provided. The third section (Section 3) discusses modeling techniques, meshing strategies, boundary conditions, and relevant equations. Described in Section 4 is a 3D numerical model of the seawall under consideration, including physics, verification, and sensitive analyses of the model. A summary of the key findings from the numerical modeling of the proposed seawall is presented in Section 5. The discussion focuses on the various parameters related to porous media and their influence on overtopping discharge. A summary of the study's main findings is presented in Section 6, which evaluates the effectiveness of the proposed approach in mitigating overtopping discharge in a system of this type.

2. Characteristics of the selected seawall

A conventional BIS is selected as a representative example, featuring a toe berm similar to that described by Shaeri and Etemad-Shahidi [8]. Layers of porous material, with a thickness denoted by t, are affixed to the seaward side of the BIS, as illustrated in Figure 1, which shows the cross-section of the model. The porous layer is assumed to be a prefabricated sand-based composite panel rather than loose sand. These panels can be mechanically fixed to the seawall face using anchors or concrete coating, allowing them to remain stable even on steep slopes.

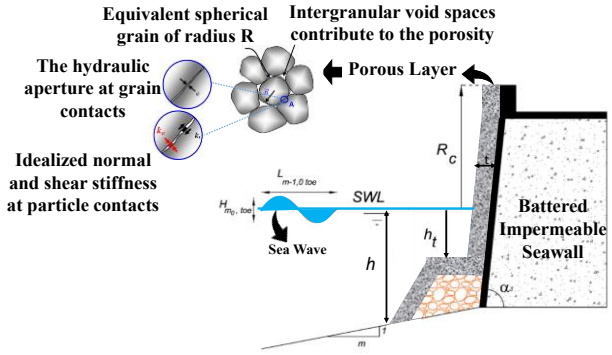

Fig. 1: Typical cross-section of a conventional BIS with a berm modified by porous layers

The model includes the following parameters: h, depth of seawater at the toe of the BIS; $H_{mo,\,toe}$, spectral wave height [34] at the toe; $L_{m\text{-}1,\,toe}$, wavelength at the toe; h_t, depth of the top level of the toe berm; R_c, elevation of the seawall crest relative to the still water level (SWL); m, foreshore seabed slope; α, slope of the seaward side of the BIS face. It is assumed that R_c is above the SWL, while h_t, the top level of the toe berm, consistently remains below the SWL. Furthermore, the idealized porous medium concepts are illustrated in the upper part of Figure 1 [35].

3. Numerical modeling

In this study, the seabed is assumed to be impenetrable, and the effects of scour are considered negligible. The porous media are assumed to undergo significant deformation. The governing equations, boundary conditions, and mesh generation procedure are described in detail in the subsequent sections.

3.1 Governing Equation

This section presents the governing equations describing flow and porous media interaction. These equations constitute the fundamental mathematical framework used to model the dynamics of fluid motion, accounting for conservation laws and the physical characteristics of the porous structure. The formulation incorporates the flow complexities through interconnected voids, critical in simulating realistic interactions between fluids and porous materials.

3.1.1. Fluid Flow

A three-dimensional numerical model has been developed to evaluate the overtopping rate of the modified BIS using the volume of fluid (VOF)-based two-phase flow model. According to the Flow-3D manual, the equations governing mass continuity and momentum are expressed as Eqs. (1-4) [36].

$$V_f \frac{\partial \rho}{\partial t} + \frac{\partial}{\partial x}(\rho u A_x) + \frac{\partial}{\partial y}(\rho v A_y) + \frac{\partial}{\partial z}(\rho w A_z) = 0 \quad (1)$$

$$\frac{\partial u}{\partial t} + \frac{1}{V_f}\left(u A_x \frac{\partial u_i}{\partial x} + v A_y \frac{\partial u_i}{\partial y} + w A_z \frac{\partial u_i}{\partial z}\right) = -\frac{1}{\rho}\frac{\partial p}{\partial x_i} + \frac{\partial g}{\partial x_i} + \frac{\partial \tau_{ij}}{\partial x_i} - b_i \quad (2)$$

where V_f is the fractional volume open to flow, A is the fractional area open to flow in x, y, and z-direction, g is the gravitational acceleration, p is the fluid pressure, x_i is the Cartesian coordinate, u_i is the velocity, t is the time, b_i is the flow losses in porous media, ρ is the fluid density, τ_{ij} is the viscous acceleration, which is presented as Eq. (3).

$$\tau_{ij} = \mu\left(\frac{\partial \langle u_j \rangle}{\partial x_i} + \frac{\partial \langle u_i \rangle}{\partial x_j}\right) - \rho \langle u_i' u_j' \rangle \quad (3)$$

where μ is the dynamic viscosity, $-\rho\langle u_i' u_j' \rangle$ is the Reynolds stress term. The Reynolds stress term can be estimated by applying the eddy-viscosity assumption (Eq. 4).

$$-\rho \langle u_i' u_j' \rangle = \mu_t\left(\frac{\partial \langle u_j \rangle}{\partial x_i} + \frac{\partial \langle u_i \rangle}{\partial x_j}\right) - \frac{2}{3}\rho \delta_{ij} k \quad (4)$$

where μ_t is the turbulent viscosity, k is the turbulence kinetic energy, and δ_{ij} is the Kronecker delta.

FLOW-3D employs various turbulence models, including k-ε, k-ω, RNG, and LES. In this study, the standard k–ε turbulence model was used, and its governing equations are presented in Eqs. (5) to (7)[37]:

$$\frac{\partial \rho k}{\partial t}+\frac{\partial \rho\langle u_i\rangle k}{\partial x_j}=\frac{\partial}{\partial x_j}\left[\left(\mu+\frac{\mu_t}{\sigma_k}\right)\frac{\partial k}{\partial x_j}\right]+\rho P_k \quad (5)$$

$$\frac{\partial \rho \varepsilon}{\partial t}+\frac{\partial \rho\langle u_i\rangle \varepsilon}{\partial x_j}=\frac{\partial}{\partial x_j}\left[\left(\mu+\frac{\mu_t}{\sigma_\varepsilon}\right)\frac{\partial k}{\partial x_j}\right]+\frac{\varepsilon}{k}(C_{\varepsilon 1}\rho P_k-C_{\varepsilon 2}\rho\varepsilon) \quad (6)$$

$$\mu_t=\rho C_\mu\frac{k^2}{\varepsilon} \quad (7)$$

The constant values of Eqs. (5) to (7) are $C_{\varepsilon 1}=1.44$, $C_{\varepsilon 2}=1.92$, $C_\mu=0.09$, $\sigma_k=1.00$, $\sigma_\varepsilon=1.30$ which are calibrated by comprehensive data fitting for a wide range of turbulent flows [38, 39].

The volume of fluid (VOF) technique was employed to calculate the free surface of the water. A function F, representing the fractional volume of water, is defined by Eq. (8) [36]. When a cell is filled with water, F equals 1; conversely, when a cell is entirely occupied by air, F equals 0. The cell contains a water-free surface for F between 0 and 1. The cell includes a water-free surface for F between 0 and 1.

$$\frac{\partial F}{\partial t}+\frac{\partial (u_i F)}{\partial x_i}=0 \quad (8)$$

3.1.2. Porous media

As previously mentioned, layers of porous media are installed on the BIS. In the porous media equation, mass conservation follows the same principles as Eq. (1), involving the development of a continuum model for porosity and applying averaging within each control volume. Based on Darcy's observations, a momentum equation for the porous media is established. According to Darcy's law, the flow resistance in the porous medium is modeled by introducing a drag term into the momentum equations. This drag term, which affects the flow velocity, is added to the right-hand side of the momentum equation (Eq. 9).

$$b=F_d.u_i \quad (9)$$

F_d is the porous media drag coefficient, and u_i is the velocity components. When a porous medium consists of coarse particles, the microscopic velocity can become significant, and the induced flow losses may be proportional to the square of the flow velocity rather than being a linear function. For Reynolds numbers greater than 10, the drag force is expressed as Eq. (10) [36].

$$F_d=-g(an+bn^2|u_i|) \quad (10)$$

where a and b are written as Eq. (11).

$$a=\alpha_F\frac{(1-n)^2}{n^3}\frac{\nu}{gD^2},\qquad b=\beta_F\frac{(1-n)}{n^3}\frac{1}{gD} \quad (11)$$

where D is a characteristic grain size diameter, α_F and β_F are dimensionless shape factors, u_i is the velocity component solved in the momentum equation, representing the seepage velocity in the porous medium, and u_i is the norm of the seepage velocity vector, and n is the porosity. The governing equations in Flow-3D are solved using the VOF-based model [40] on a structured Cartesian mesh. The transient term is typically discretized using a first-order implicit scheme for stability, while the advection term uses a second-order accurate scheme for advection to minimize numerical diffusion. Time advancement is performed using a fully implicit first-order scheme, which provides unconditional stability and allows relatively large time steps without violating numerical stability criteria. The pressure-velocity coupling is handled using a robust implicit solver based on strongly implicit procedures [36, 41].

3.2. Boundary Conditions

A computational domain was defined around the modified BIS (see Figure 2). Boundary conditions were specified for each aspect of the domain, denoted as follows: (1) WV: related to inflow, encompassing waves and currents that can enter or leave the domain; (2) O: related to outflow; (3) S: lateral boundaries, referred to as symmetry boundaries; (4) W: solid boundaries. Regarding the boundary conditions, the tangential shear stress at the free surface was set to zero, while the normal stress was equilibrated with atmospheric pressure. Indeed, the free surface is treated according to Flow-3D's VOF formulation, where the gauge pressure is set to zero, corresponding to atmospheric pressure. The tangential shear stress at the free surface is assumed to be zero, neglecting viscous effects in the air phase. This approach is consistent with standard practice in VOF-based free-surface flow modeling.

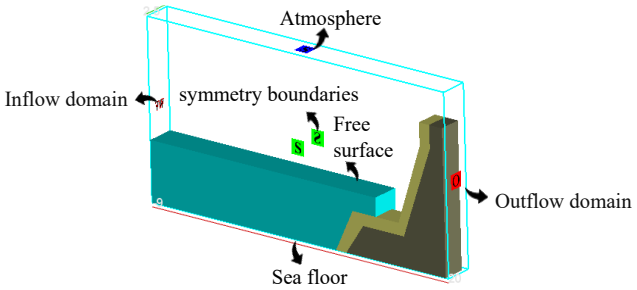

Fig. 2. Schematic of boundary conditions for different parts of the computational domain

For the wave boundary, both the position of the free surface and the velocity at the boundary were specified according to governing wave theory. All solid surfaces, including the seafloor and the bottom of the BIS, were subjected to the no-slip boundary condition. Additionally, turbulent energy and dissipation at the free surface boundary were set to zero in the normal direction.

3.3. Wave Simulation

In this study, wave propagation and its interaction with the seawall were simulated by directly solving the three-

dimensional Reynolds-Averaged Navier–Stokes (RANS) equations coupled with the VOF method implemented in FLOW-3D. This modeling approach fully resolves the hydrodynamic field and nonlinear free-surface deformation throughout the computational domain, rather than relying on spectral or empirical wave formulations.

Regular waves were generated at the inlet based on the fifth-order Stokes theory by specifying the wave height, period, and water depth [34, 42]. To minimize wave reflection, three sets of numerical wave-absorption boundary conditions were applied near the outlet using the dispersion relation and a digital filtering technique to enforce outgoing velocities opposite to the incoming waves.

The wave parameters (height, period, and phase) and the selected wave theory were defined in the *WaveDict* file. At the same time, all generation and absorption boundary conditions were prescribed in the *0* folder for the velocity field.

3.4. *Mesh sensitivity analysis*

Structured meshes were used in this study, and the volume elements were arranged logically. Figure 3 illustrates the definition of a mesh plane.

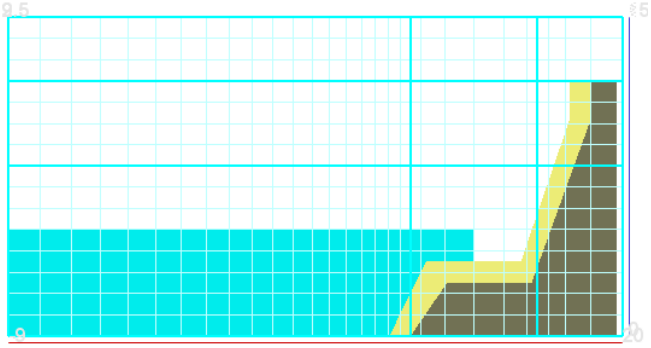

Fig. 3. Creating the mesh for modeling with Flow-3D

A mesh sensitivity analysis was conducted to ensure reliable numerical solutions of the governing equations. The transient simulation was performed for 55 seconds until a quasi-steady state was reached. A convergence study was carried out to determine an appropriate mesh density. Various square mesh sizes and corresponding counts, detailed in Table 1, were evaluated by calculating the overtopping rate for each configuration. The results are shown in Figure 4. During these tests, mesh sizes of 0.5 m and 1.0 m produced consistent outcomes, and given the lower computational cost and reduced simulation time, a maximum mesh size of 1.0 m was selected for subsequent analyses.

Notably, a slightly lower accuracy was observed for the mesh size of 0.25 m. This suggests that excessive mesh refinement can reduce the local Courant number and make the solver overly sensitive to turbulence gradients near the free surface, leading to minor oscillations in the free-surface and turbulence fields. Furthermore, without a proportional reduction in the time step, additional mesh refinement does not necessarily improve accuracy and may even introduce numerical artifacts [43].

Table 1. The number and sizes of meshes used for sensitivity analysis

Model	Δx (m)	Δy (m)	Δz (m)	Grid number
1	0.25	0.25	0.25	90000.0
2	0.50	0.50	0.50	11600.0
3	1.00	1.00	1.00	2175.00
4	2.00	2.00	2.00	288.000
5	3.00	3.00	3.00	100.000
6	4.00	4.00	4.00	32.0000

Notably, a slightly lower accuracy was observed for the mesh size of 0.25 m. This suggests that excessive mesh refinement can reduce the local Courant number and make the solver overly sensitive to turbulence gradients near the free surface, leading to minor oscillations in the free-surface and turbulence fields. Furthermore, without a proportional reduction in the time step, additional mesh refinement does not necessarily improve accuracy and may even introduce numerical artifacts [43].

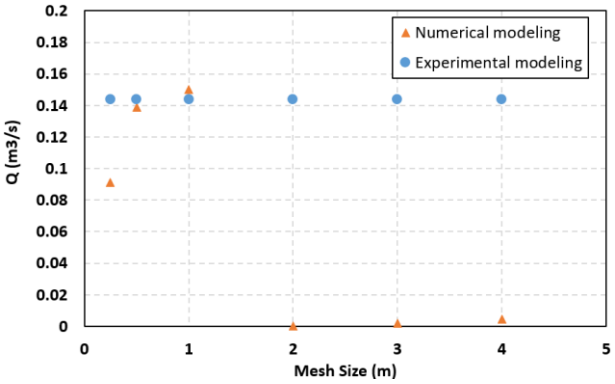

Fig. 4. Comparison of the Mesh convergence investigation between the Shaeri and Etemad-Shahidi [8] formula and numerical modeling

4. Validation of Numerical Model

To validate the numerical model, a series of simulations was conducted for an impermeable seawall without any porous layers, focusing on two key parameters: spectral wave height (H_{mo}) and the crest elevation of the seawall relative to the still water level (R_c). The computational mesh employed a maximum element size of 1 m with an average surface roughness coefficient of 0.02, while all remaining conditions adhered to the experimental setup of Shaeri and Etemad-Shahidi [8]. The first set of simulations investigated the model's sensitivity to wave height by varying H_{mo} across five levels (1.0, 1.5, 2.0, 2.25, and 2.43 m), keeping *Rc* constant at 6 m. In the second set, R_c was systematically altered (2.0 to 6.0 m) while holding H_{mo} constant at 2.0 m to assess the model's response to structural elevation. Overtopping discharges were extracted from the numerical model and

validated using the formula proposed by Shaeri and Etemad-Shahidi [8]. Notably, no CLASH project data were used in this validation.

The comparison results in Figures 5 and 6 demonstrate a consistently strong agreement between the numerical and experimental findings. For variations in H_{mo}, the percentage agreement exceeded 94% across all cases, indicating the model's high capability in capturing wave dynamics and overtopping behavior under different sea states.

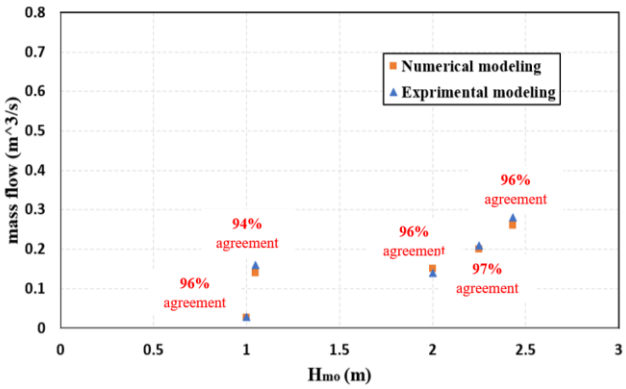

Fig. 5. Comparison of H_{mo} between the Shaeri and Etemad-Shahidi [8] formula and numerical modeling

Similarly, Figure 6 shows that agreement for varying R_c values is above 92% in all cases. Overall, the validation process confirms the robustness and accuracy of the numerical model for predicting wave overtopping over impermeable seawalls.

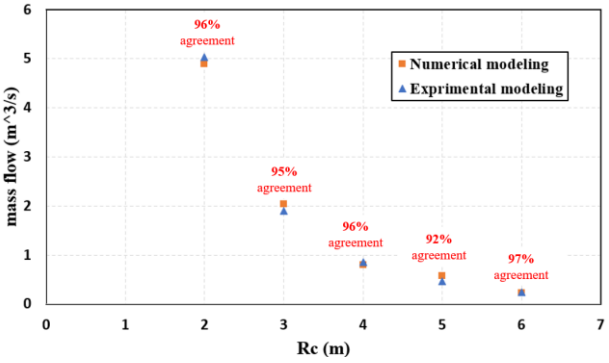

Fig. 6. Comparison of Rc between the Shaeri and Etemad-Shahidi [8] formula and numerical modeling

5. Results and discussion

5.1. Effect of porous media on overtopping

Building upon the validated numerical framework discussed in the previous section, this part presents the simulation results for the impermeable seawall modified by adding porous layers. The physical and geometric properties of the porous media used in the simulations are detailed in Table 2. To comprehensively assess the influence of porous media, three parametric scenarios—A, B, and C—were defined as follows:

1. By varying the thickness of the porous layer while keeping another parameter constant, scenario A investigates the effect of the porous layer thickness.
2. In scenario B, the sand grain size is changed within the layer while maintaining the other parameters unchanged.
3. In scenario C, the porosity percentages within the layer are modified to examine the effects of porosity.

These scenarios concerning the reduction of wave overtopping are discussed in the following sections. Notably, the scenarios were selected to investigate the effect of varying wall thickness and porosity on wave overtopping. While some combinations may require additional stabilization measures in practice, all configurations are considered feasible under controlled engineering conditions.

Scenario A: Effect of Porous Layer Thickness

Scenario A focuses on evaluating the impact of porous layer thickness on the hydrodynamic performance of the BIS-coated seawall system. In this scenario, a series of numerical simulations was carried out in which the seawall was overlaid with porous layers of varying thicknesses—specifically 0.4 m, 0.6 m, 1.0 m, and 2.0 m. The primary goal was to investigate how increasing the thickness of the porous medium affects the overtopping-related flow rate and energy dissipation.

Table 2. Various scenarios for porous layers attached to the BIS

Properties	Scenarios		
	A	B	C
Poisson's ratio	0.333	0.333	0.333
Fluid kinematic viscosity (m^2/s)	1.12×10^{-6}	1.12×10^{-6}	1.12×10^{-6}
Pore fluid compression coefficients (m^2/N)	4.35×10^{-10}	4.35×10^{-10}	4.35×10^{-10}
Turbulent drag coefficient	0.2	0.2	0.2
Added mass coefficient	0.015	0.015	0.015
Elastic solid density (kg/m^3)	2650	2650	2650
Fluid density (kg/m^3)	1010	1010	1010
Shear modulus (N/m^2)	5×10^4	5×10^4	5×10^4
Intrinsic Permeability (m^2)	2.28×10^{-8}	2.28×10^{-8}	2.28×10^{-8}
Thickness (m)	0.40 0.60 1.00 2.00	0.40	0.40
Grain Size (mm)	2.00	0.20 0.50 1.00 2.00	2.00
Porosity Percentage (%)	40	40	20 30 40 50

The simulation results (Figure 7 and Table 3) reveal a clear and consistent inverse relationship between the thickness of the porous layer and the mass flow rate through the system. As the layer becomes thicker, the flow rate decreases significantly. For instance, with a porous layer of just 0.4 m, the flow rate dropped to 0.056 m³/s, marking a 62.6% reduction relative to the baseline case without any porous media (0.15 m³/s). Increasing the thickness to 2.0 m resulted in a dramatic flow reduction to 0.007 m³/s, equating to a 95.3% decrease.

Table 3. The rate of flow in Scenario A

Thickness (m)	Flow rate in Scenario A (m^3/s)	The flow rate in BIS without porous layers (m^3/s)	Reducing percentages (%)
0.40	0.056	0.15	62.6
0.60	0.041	0.15	72.6
1.00	0.018	0.15	88.0
2.00	0.007	0.15	95.3

This trend can be attributed to enhanced wave energy dissipation and increased internal flow resistance within the porous structure. A thicker porous layer offers a greater volume for turbulent mixing, frictional losses, and pore-scale interactions, which collectively slow down the momentum of incoming waves and reduce the overtopping discharges. Additionally, thicker layers extend the water's path, increasing the contact time between the fluid and the internal matrix, further amplifying energy losses.

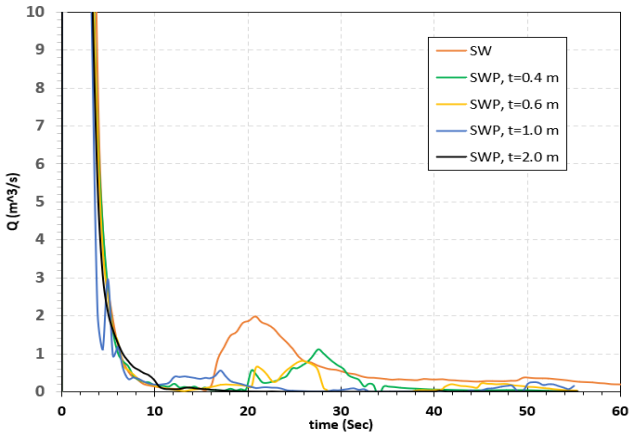

Fig.7. The trend of changes in mass flow rate per unit time over 55 seconds with various porous layer thicknesses (SW: abbreviation for seawall without porous layer and SWP: abbreviation for seawall with porous layer), Scenario A

Figure 7 illustrates the temporal variation of mass flow rate (Q) over 55 seconds for different porous layer thicknesses applied to the seawall (SWP), compared with the reference impermeable seawall without porous media (SW). In the initial phase (0–5 seconds), all curves show a sharp and pronounced flow rate peak, representing the incident wave's initial impact and the onset of overtopping. During this short interval, the flow rates are nearly identical across all cases, suggesting that the influence of the porous layers is minimal during the first wave encounter, as the system has not yet reached dynamic equilibrium and the momentum of the incoming wave dominates the response.

Following this peak, a rapid decline in mass flow rate is observed for all cases. However, the rate and nature of this decline differ significantly with varying porous layer thicknesses. The seawall without any porous coating (SW – orange line) maintains the highest flow rates throughout the simulation, indicating limited energy dissipation and persistent overtopping. In contrast, the seawalls with porous layers exhibit a marked reduction in overtopping, with flow rates decreasing as the thickness of the porous media increases.

Notably, the SWP with a 0.4 m and 0.6 m porous layer (green and yellow lines) shows moderate reductions. However, some fluctuations persist in the mid-time window (20–40 seconds), reflecting residual wave energy and possible internal recirculation. Overtopping is significantly diminished in thicker configurations (1.0 m and 2.0 m – blue and black lines). The 2.0 m case, in particular, demonstrates a consistently low and smooth profile, with mass flow rates approaching negligible levels after approximately 10 seconds. This indicates that the thick porous layer effectively absorbs and dissipates most of the wave energy, stabilizing the system and limiting the mass exchange.

Moreover, the figure reveals that increasing the thickness of the porous layer enhances the damping effect, especially beyond 1.0 m. At this threshold, the wave energy is sufficiently attenuated to prevent further substantial overtopping, confirming the role of porous media in enhancing the hydrodynamic performance of coastal defences.

Scenario B: Effect of Porous Layer Grain Sizes

Scenario B examined the influence of grain size on wave overtopping reduction with grain sizes of 0.2 mm, 0.5 mm, 1 mm, and 2 mm (see Table 2, Scenario B). To isolate the effect of grain size, other critical parameters, such as thickness, porosity, intrinsic permeability, and shear modulus, were kept constant throughout the analysis. Table 4 summarizes the results based on the simulations, and Figure 8 represents them graphically. The numerical analysis indicates that sand particle sizes between 0.2 mm and 1 mm produced similar levels of wave overtopping reduction without exhibiting any significant differences. There was, however, a noticeable improvement in wave overtopping reduction when the grain size was increased to 2 mm, suggesting that larger particles may enhance the damping effect of the porous layer.

Table 4. The rate of flow reduction at the end of the seawall with a porous layer of different particle diameters, Scenario B

Diameters (mm)	Flow rate in Scenario A (m^3/s)	The flow rate in BIS without porous layers (m^3/s)	Reducing percentages (%)
0.20	0.064	0.15	57.33
0.50	0.064	0.15	57.33
1.00	0.064	0.15	57.33
2.00	0.056	0.15	62.60

Figure 8 further illustrates that for fine particle sizes (0.2–1 mm). According to this figure, during the early stage of the simulation (0–5 seconds), all scenarios display a sharp, nearly identical peak in flow rate caused by the initial wave impact. This indicates that the grain size of the porous medium has minimal effect during the first overtopping event, as the wave's inertia and force dominate the dynamics before significant interaction with the porous structure occurs.

However, shortly after this peak, distinct differences emerge among the curves. For fine-grained configurations (0.2 mm, 0.5 mm, and 1.0 mm—blue, light blue, and black lines), the flow rate declines sharply, and overtopping is significantly reduced in the early moments, reflecting effective energy dissipation. Despite this promising initial performance, these finer grains exhibit increasing fluctuations and secondary peaks in the mid-time window (around 10–30 seconds), with some flow rates temporarily exceeding those of the baseline case (SW). This suggests that smaller grain sizes may initially suppress overtopping. Still, they might enable delayed flow pathways or internal pressure buildup, thus diminishing their long-term effectiveness under continuous wave forcing.

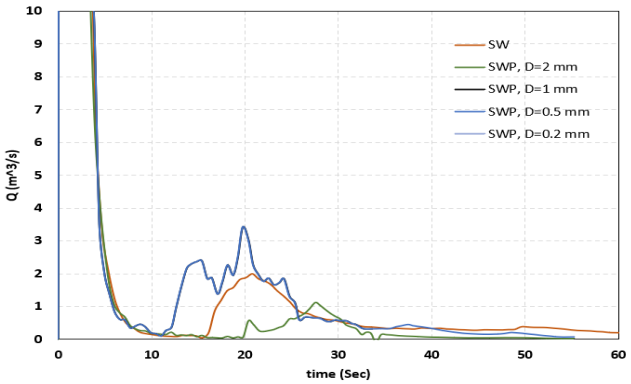

Fig. 8. The trend of changes in flow rate per unit time over 55 seconds with various porous layer diameters (SW: abbreviation for seawall without porous layer, and SWP: abbreviation for seawall with porous layer)

In contrast, the SWP with a 2.0 mm grain size (green line) demonstrates consistently superior performance. After the initial decline, the flow rate remains notably lower than the other configurations, with fewer fluctuations and a more stabilized profile throughout the 55-second simulation. This indicates that coarser grains are more effective at maintaining sustained energy dissipation and flow resistance, likely due to enhanced interstitial flow pathways and reduced pressure buildup caused by permeability.

This observation is further supported by Table 4, which quantifies the percentage reduction in flow rate compared to the baseline. While the finer grains (0.2–1.0 mm) achieved an identical flow reduction rate of 57.33%, the 2.0 mm configuration showed a higher reduction of 62.60%. Although the differences in early-stage performance are subtle, their cumulative effect over time becomes significant.

Overall, the results suggest that finer grain sizes are effective for immediate overtopping reduction but are less capable of sustaining that reduction under prolonged wave action. Conversely, coarser grains such as 2.0 mm offer advantages both in immediate and long-term performance. These findings highlight the importance of optimizing grain size in porous media to enhance short-term damping and long-term stability in wave energy dissipation. Such insights are crucial for designing advanced coastal defense systems with porous components tailored for durable and rapid performance under wave attack.

Scenario C: Effect of Porous Layer Porosity

To evaluate the effect of porosity in the porous layer on wave overtopping behavior, a series of numerical simulations were carried out using four different porosity values: 20%, 30%, 40%, and 50% (Scenario C in Table 2). In these simulations, the porous layer thickness was fixed at 40 cm. Also, other material characteristics—including grain size, intrinsic permeability, and shear modulus—remained constant. This setup allowed for an isolated investigation of porosity as the sole varying parameter.

The simulation results in Table 5 and Figure 9 demonstrate a clear correlation between increasing porosity and enhanced overtopping reduction. As porosity rose from 20% to 50%, the peak and cumulative overtopping discharges diminished significantly. In particular, the flow reduction reached 67.30% in the case of 50% porosity, compared to the base case without a porous layer, indicating a steady improvement in performance as porosity increased.

Figure 9 illustrates all porosity levels' time-dependent flow rate (Q). Initially, all curves exhibit a sharp peak, consistent with the impact of the first wave front. However, the dissipation behavior diverges soon after. The SWP with lower porosity (20% – yellow line) shows a higher and more prolonged overtopping event than the more porous layers. The flow rate decreases rapidly as porosity increases to 30%, 40%, and 50%. It remains consistently lower throughout the simulation, demonstrating the porous layer's improved

capacity to dissipate wave energy and delay or suppress overtopping.

Notably, the SWP with 50% porosity (black line) presents the lowest flow rate across almost the entire 55-second duration, indicating sustained and superior performance in dampening overtopping discharge. This outcome can be attributed to the greater void space in higher porosity materials, which facilitates enhanced absorption and internal flow diffusion of wave energy, thereby reducing the kinetic energy available to cause overtopping. The results underscore the critical role of porosity in the design of effective porous layers. Higher porosity contributes to a greater initial reduction in overtopping discharge and ensures a faster and more stable decline in flow rate over time.

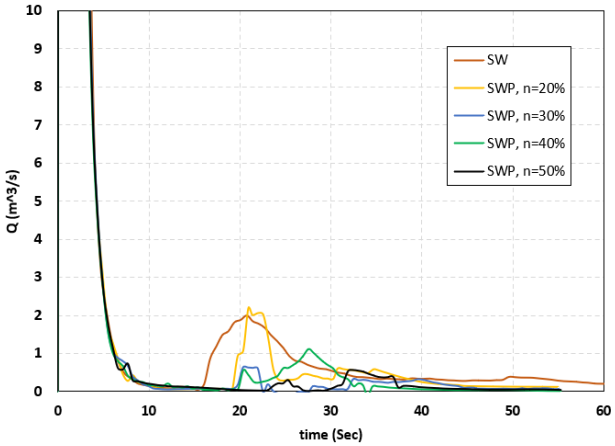

Fig. 9. The trend of changes in mass flow rate per unit time over 55 seconds with various porous layers and different porous percentages (SW: abbreviation for seawall without porous layer, and SWP: abbreviation for seawall with porous layer)

Table 5. The rate of flow reduction at the end of the seawall with a porous layer of different porosities, Scenario C

Porous percentages (%)	Flow rate in Scenario A (m^3/s)	The flow rate in BIS without porous layers (m^3/s)	Reducing percentages (%)
20	0.060	0.15	60.00
30	0.059	0.15	60.60
40	0.056	0.15	62.60
50	0.049	0.15	67.30

6. Conclusions

The main objectives of the seawall are to protect coastal areas from the destructive effects of waves, human habitation, conservation, and leisure activities from the action of currents, tides, storms, or tsunamis. However, wave overtopping remains a critical hydraulic parameter that can compromise the performance and stability of these structures, often leading to severe structural damage and economic losses. In this study, we proposed a practical solution to mitigate wave overtopping, introducing a porous sandy layer on an impermeable seawall. The numerical modeling is conducted using a finite volume method and calibrated with experimental data, investigating the effects of porous layer parameters on flow rate and overtopping discharge. The results demonstrated the significant potential of the porous layer to enhance seawall performance, as summarized below:

(1) *A porous layer substantially reduces the seawall's water volume and flow rate compared to the scenario without a porous layer, demonstrating its effectiveness in mitigating wave overtopping.*

(2) *Layer thickness emerged as a critical parameter. A porous layer with a thickness of at least 40 cm reduced the flow rate by over 60%, and further increases in thickness brought the mass flow rate close to zero, showcasing the importance of optimizing layer dimensions*

(3) *Porosity significantly influenced flow rate reduction. A porosity of 20% achieved a 60% reduction in flow rate, while increasing porosity to 50% improved the reduction to 67.3%, indicating the role of pore structure in enhancing energy dissipation.*

(4) *The numerical research shows that the grain size also impacts the performance of the structure's behavior under the destructive effects of waves, the action of currents, tides, and tsunamis. While grain sizes between 0.2 mm and 1 mm produced similar reductions (~33.57%), a grain size of 2 mm significantly enhanced the reduction, achieving 62.6%. The grain size of 2 mm highlights the importance of considering particle size distribution in porous layer design*

(5) *In all scenarios, the porous layer accelerated the reduction in mass flow rate, allowing it to reach its minimum value more quickly than without a porous layer.*

Collectively, these outcomes underscore the value of porous layers as a straightforward and feasible method for enhancing the resilience of seawalls. By carefully optimizing parameters such as thickness, porosity, and grain size, engineers can significantly reduce overtopping discharge, ultimately improving the reliability and sustainability of coastal protection systems.

☑ *Recommendations for Future Work*

While this study provides valuable insights into the effectiveness of porous layers, several areas remain open for further investigation:

- Investigating the long-term stability and durability of the porous layer under real-world conditions, including sediment transport, biofouling, and erosion, will provide a more comprehensive understanding of its practical application.

- Exploring alternative materials for the porous layer, such as eco-friendly or recycled materials, may improve sustainability while maintaining performance.
- Field experiments in real coastal environments should be conducted to validate numerical findings and account for environmental factors that may not be fully captured in simulations.
- By addressing these areas, future studies can build upon the foundation established here to optimize and implement porous layer technology in coastal defence systems, ensuring more effective and sustainable solutions for wave overtopping mitigation.

Acknowledgements

The authors would like to express their sincere gratitude to the Department of Civil Engineering at the University of Hormozgan, Bandar Abbas, University of Science and Technology of Mazandaran, Behshahr, Iran, and the Department of Civil Engineering, Sardar Vallabhbhai National Institute of Technology, Surat, India, for providing the necessary facilities and resources that enabled the successful completion of this study. We also appreciate the time and helpful comments of the editorial and peer-review teams, which significantly improved the quality of this manuscript.

References

[1] Koosheh, A., Etemad-Shahidi, A., Cartwright, N., Tomlinson, R., and van Gent, M. R., "Individual wave overtopping at coastal structures: A critical review and the existing challenges," *Applied Ocean Research,* vol. 106, p. 102476, 2021.

[2] Owen, M., "Design of seawalls allowing for wave overtopping," *Report Ex,* vol. 924, p. 39, 1980.

[3] Goda, Y., *Random seas and design of maritime structures*. World Scientific Publishing Company, 2010.

[4] van der Meer, J. W., "Wave run-up and wave overtopping at dikes," *Wave forces on inclined and vertical structures, ASCE,* 1995.

[5] Etemad-Shahidi, A., Shaeri, S., and Jafari, E., "Prediction of wave overtopping at vertical structures," *Coastal Engineering,* vol. 109, pp. 42-52, 2016.

[6] Pillai, K., Etemad-Shahidi, A., and Lemckert, C., "Wave overtopping at berm breakwaters: Experimental study and development of prediction formula," *Coastal Engineering,* vol. 130, pp. 85-102, 2017.

[7] Williams, H. E., Briganti, R., Romano, A., and Dodd, N., "Experimental analysis of wave overtopping: A new small scale laboratory dataset for the assessment of uncertainty for smooth sloped and vertical coastal structures," *Journal of Marine Science and Engineering,* vol. 7, no. 7, p. 217, 2019.

[8] Shaeri, S. and Etemad-Shahidi, A., "Wave overtopping at vertical and battered smooth impermeable structures," *Coastal Engineering,* vol. 166, p. 103889, 2021.

[9] Chen, H., Yuan, J., Cao, D., and Liu, P. L.-F., "Wave overtopping flow striking a human body on the crest of an impermeable sloped seawall. Part II: Numerical modelling," *Coastal Engineering,* vol. 168, p. 103892, 2021.

[10] Cao, D., Yuan, J., Chen, H., Zhao, K., and Liu, P. L.-F., "Wave overtopping flow striking a human body on the crest of an impermeable sloped seawall. Part I: Physical modeling," *Coastal Engineering,* vol. 167, p. 103891, 2021.

[11] Kobayashi, N. and Wurjanto, A., "Wave overtopping on coastal structures," *Journal of Waterway, Port, Coastal, and Ocean Engineering,* vol. 115, no. 2, pp. 235-251, 1989.

[12] Hubbard, M. E. and Dodd, N., "A 2D numerical model of wave run-up and overtopping," *Coastal Engineering,* vol. 47, no. 1, pp. 1-26, 2002.

[13 Xiao, H., Huang, W., and Tao, J., "Numerical modeling of wave overtopping a levee during Hurricane Katrina," *Computers & Fluids,* vol. 38, no. 5, pp. 991-996, 2009.

[14] Tsung, W.-S., Hsiao, S.-C., and Lin, T.-C., "Numerical simulation of solitary wave run-up and overtopping using Boussinesq-type model," *Journal of Hydrodynamics,* vol. 24, no. 6, pp. 899-913, 2012.

[15] Yuan, T., Wang, X., Qu, K., and Zhang, L., "Hydrodynamic Loads and Overtopping Processes of a Coastal Seawall under the Coupled Impact of Extreme Waves and Wind," *Journal of Marine Science and Engineering,* vol. 11, no. 11, p. 2087, 2023.

[16] CHIWATA, M., HASUMI, K., ODA, Y., and ITO, K., "NUMERICAL STUDY ON WAVE OVERTOPPING AND OVERFLOW THROUGH SEAWALL LINE IN STORM SURGE," *土木学会論文集 B2 (海岸工学)(Web),* vol. 76, no. 2, pp. 109-114, 2020.

[17] Pu, J. H. and Shao, S., "Smoothed particle hydrodynamics simulation of wave overtopping characteristics for different coastal structures," *The Scientific World Journal,* vol. 2012, no. 1, p. 163613, 2012.

[18] Chen, W., Warmink, J., Van Gent, M., and Hulscher, S., "Numerical modelling of wave overtopping at dikes using OpenFOAM®," *Coastal engineering,* vol. 166, p. 103890, 2021.

[19] Yamamoto, T., "On the response of a Coulomb-damped poroelastic bed to water waves," *Marine Georesources & Geotechnology,* vol. 5, no. 2, pp. 93-130, 1983.

[20] Lee, T., Tsai, C., and Jeng, D., "Ocean waves propagating over a coulomb-damped poroelastic seabed of finite thickness: An analytical solution," *Computers and Geotechnics,* vol. 29, no. 2, pp. 119-149, 2002.

[21] Song, C., "Dynamic response of poro-elastic bed to water waves," PhD Thesis, National Taiwan University, Taiwan, ROC, 1993.

[22] Jeng, D.-S. and Cha, D., "Effects of dynamic soil behavior and wave non-linearity on the wave-induced pore pressure and effective stresses in porous seabed," *Ocean Engineering,* vol. 30, no. 16, pp. 2065-2089, 2003.

[23] Zhou, X.-L., Xu, B., Wang, J.-H., and Li, Y.-L., "An analytical solution for wave-induced seabed response in a multi-layered poro-elastic seabed," *Ocean Engineering,* vol. 38, no. 1, pp. 119-129, 2011.

[24] Lan, Y.-J. and Lee, J.-F., "On waves propagating over a submerged poro-elastic structure," *Ocean Engineering,* vol. 37, no. 8-9, pp. 705-717, 2010.

[25] Lan, Y.-J., Hsu, T.-W., Lai, J.-W., Chang, C.-C., and Ting, C.-H., "Bragg scattering of waves propagating over a series of poro-elastic submerged breakwaters," *Wave Motion,* vol. 48, no. 1, pp. 1-12, 2011.

[26] Lan, Y.-J., Hsu, T.-W., and Chen, C.-Y., "ANALYSIS OF WAVE INTERACTION WITH SUBMERGED ADJACENT PORO-ELASTIC BREAKWATERS," *Coastal Engineering Proceedings,* vol. 1, no. 33, p. 31, 2012.

[27] Lan, Y.-J., Kuo, Y.-S., Hsu, T.-W., and Chen, C.-Y., "On waves propagating over two submerged closely spaced poroelastic breakwaters," *Proceedings of the Institution of Mechanical*

Engineers, Part M: Journal of Engineering for the Maritime Environment, vol. 227, no. 3, pp. 295-308, 2013.
[28] Emami, A. and Gharabaghi, A. R. M., 2018, "REDUCING HEAVE RESPONSE AMPLITUDE OPERATOR OF A SEMI-SUBMERSIBLE PLATFORM USING PORO-ELASTIC PLATES," in *The 13th Int Conf on Coasts, Ports & Marine Structures*, 2018, pp. 229-230.
[29] Lan, Y. and Hsu, T., "Analytical Solution for Wave Interaction with a Stack-type Double-layer Composite Poroelastic Submerged Structure," *Applied Mathematical Sciences,* vol. 8, no. 37, pp. 1799-1816, 2014.
[30] Emami, A. and Gharabaghi, A. R. M., "Application of poroelastic layers in a semi-submersible platform: Devising an efficient heave motion response reduction method," *Ocean engineering,* vol. 201, p. 107148, 2020.
[31] Emami, A., Pourjafari, N., and Parghi, A., "Effect of porous SBR composites on mitigating the heave motion response of a semi-submersible platform," *Ocean Engineering,* vol. 295, p. 116856, 2024.
[32] Mohammadi, P., Emami, A., Gharabaghi, A. R. M., Tahmooresi, S., Chenaghlou, M. R., and Ghavifekr, H. B., "Evaluation of RAOs of a semi-submersible platform using field measurements: A full-scale model in Caspian sea environmental conditions," *Marine Structures,* vol. 91, p. 103467, 2023.
[33] Hieu, P. D. and Vinh, P. N., "Numerical study of wave overtopping of a seawall supported by porous structures," *Applied Mathematical Modelling,* vol. 36, no. 6, pp. 2803-2813, 2012.
[34] Emami, A. and Karimirad, M., "Further development of offshore floating solar and its design requirements," *Marine Structures,* vol. 100, p. 103730, 2025.
[35] Selvadurai, A. and Suvorov, A., "Poroelastic properties of rocks with a comparison of theoretical estimates and typical experimental results," *Scientific Reports,* vol. 12, no. 1, p. 10975, 2022.
[36] Razavi, A. R. and Ahmadi, H., "FLOW-3D," *Civil Engineering Journal,* vol. 3, no. 10, 2017.
[37] Scott-Pomerantz, C. D., "The k-epsilon model in the theory of turbulence," University of Pittsburgh, 2004.
[38] Rodi, W., *Turbulence models and their application in hydraulics*. Routledge, 2017.
[39] Launder, B. E. and Spalding, D. B., 1983. "The numerical computation of turbulent flows," in *Numerical prediction of flow, heat transfer, turbulence and combustion*: Elsevier, pp. 96-116.
[40] Hirt, C. W. and Nichols, B. D., "Volume of fluid (VOF) method for the dynamics of free boundaries," *Journal of computational physics,* vol. 39, no. 1, pp. 201-225, 1981.
[41] Patankar, S., *Numerical heat transfer and fluid flow*. CRC press, 2018.
[42] Rezaei, F., Tajziehchi, M., Soltanpour, M., and Emami, A., 2014, "Prediction of wave characteristics in Persian Gulf within Qeshm and Hormoz Islands using swan wave model," in *International Conference on Coasts, Ports and marine Structures*, 2014.
[43] Qu, S., Liu, S., and Ong, M. C., "An evaluation of different RANS turbulence models for simulating breaking waves past a vertical cylinder," *Ocean Engineering,* vol. 234, p. 109195, 2021.